

The Amyloid Precursor Protein (APP) Family Members are Key Players in S-adenosylmethionine Formation by MAT2A and Modify *BACE1* and *PSEN1* Gene Expression-Relevance for Alzheimer's Disease*

Andreas Schrötter‡, Kathy Pfeiffer‡, Fouzi El Magraoui§, Harald W. Platta§, Ralf Erdmann§, Helmut E. Meyer¶, Rupert Egensperger||, Katrin Marcus‡**, and Thorsten Müller‡‡**

Central hallmark of Alzheimer's disease are senile plaques mainly composed of β -amyloid, which is a cleavage product of the amyloid precursor protein (APP). The physiological function of APP and its family members APLP1 and APLP2 is poorly understood. In order to fill this gap, we established a cell-culture based model with simultaneous knockdown of all members of the family. A comprehensive proteome study of the APP/APLP1/APLP2 knockdown cell lysates versus controls revealed significant protein abundance changes of more than 30 proteins. Targeted validation of selected candidates by immunoblotting supported the significant down-regulation of the methionine adenosyltransferase II, alpha (MAT2A) as well as of peroxiredoxin 4 in the knockdown cells. Moreover, MAT2A was significantly down-regulated at the mRNA level as well. MAT2A catalyzes the production of S-adenosylmethionine from methionine and ATP, which plays a pivotal role in the methylation of neurotransmitters, DNA, proteins, and lipids. MAT2A-dependent significant up-regulation of S-adenosylmethionine was also detectable in the knockdown cells compared with controls. Our results point to a role of the APP family proteins in cellular methylation mechanisms and fit to findings of disturbed S-adenosylmethionine levels in tissue and CSF of Alzheimer disease patients versus controls. Importantly, methylation plays a central role for neurotransmitter generation like acetylcholine pointing to a crucial relevance of our findings for Alzheimer's disease. In addition, we identified differential gene expression of

BACE1 and *PSEN1* in the knockdown cells, which is possibly a consequence of MAT2A deregulation and may indicate a self regulatory mechanism. *Molecular & Cellular Proteomics* 11: 10.1074/mcp.M112.019364, 1274–1288, 2012.

The amyloid precursor protein (APP)¹ is a species-conserved integral membrane protein, which is expressed in many tissues. A role for APP has been suggested in neurite outgrowth and synaptogenesis, protein trafficking along axons, cell adhesion, calcium metabolism, and signal transduction (reviewed in (1, 2)). During its life cycle, APP is cleaved into various fragments mediating different functions. Next to A β (and the p3 fragment), extracellular soluble fragments (sAPP α or sAPP β), and intracellular fragments (APP intracellular domain, AICD) are generated. After sequential β - and

¹ The abbreviations used are: APP, amyloid precursor protein; ACIN1, apoptotic chromatin condensation inducer in the nucleus; AD, Alzheimer's disease; AICD, amyloid precursor protein intracellular domain; APLP1, amyloid precursor-like protein 1; APLP2, amyloid precursor-like protein 2; ASA, amino acid analysis; A β , amyloid beta; BACE1, β APP cleaving enzyme 1; BAX, BCL-2 associated X protein; BCAP31, B-cell receptor-associated protein 31; BCLAF1, BCL-2-associated transcription factor 1; ERK1/, extracellular signal regulated protein kinase 1/2 (ERK1/2); FCS, fetal calf serum; IPA, Ingenuity Pathway Analysis; JNK, c-Jun-N-terminal kinase; MAT, methionine adenosyltransferase; MAT2A, methionine adenosyltransferase II, alpha; MEM, Minimum Essential Medium; NF κ B, nuclear factor kappa-light-chain-enhancer of activated B cells; p38 MAPK, p38 mitogen-activated protein kinases; PARP1, poly (ADP ribose) polymerase 1; PBS, phosphate buffered saline; PFA, paraformaldehyde; PRDX4, peroxiredoxin 4; PS, penicillin/streptomycin; PSEN1, presenilin1; qPCR, real-time polymerase chain reaction; RPN1, dolichyl-diphosphooligosaccharide-protein glycosyltransferase; RPS23, 40S ribosomal protein S23; SAM, S-adenosylmethionine; SOCs, store operated channels; STRING, Search Tool for the Retrieval of Interacting Genes/Proteins EMBL Institute; TRPC1, C-type transient receptor potential.

From the ‡Functional Proteomics, Medizinisches Proteom-Center, Ruhr-University Bochum, D-44801 Bochum, Germany; §Institute of Physiological Chemistry, System Biochemistry, Ruhr-University Bochum, D-44780 Bochum, Germany; ¶Medizinisches Proteom-Center, Ruhr-University Bochum, D-44801 Bochum, Germany; ||Center for Neuropathology and Prion Research, Ludwig-Maximilians-University Munich, D-81377 Munich, Germany

Received April 3, 2012, and in revised form, August 1, 2012

Published, MCP Papers in Press, August 9, 2012, DOI 10.1074/mcp.M112.019364

γ -secretase cleavage, the originating sAPP β is suggested to transmit a toxic signal via interaction to the death receptor 6 (3). AICD was reported to act as a regulator of gene expression (4). Sequential cleavage through α - and γ -secretase activity results in the generation of the putatively neuroprotective fragment sAPP α as well as AICD (5). The majority of these results were derived from over-expression cell culture models which were often criticized to be artificial. Knockdown or knockout models are believed to be more descriptive when studying the physiological function of APP. APP is a member of a large gene family including the amyloid precursor-like proteins, termed APLP1 and APLP2, which are processed in a similar fashion (6). Resulting from this redundancy, the simultaneous knockdown (knockout) of two or all family members is indicated to study APP family dependent mechanisms.

Mice lacking all three APP family members die shortly after birth and reveal a strong cortical dysplasia (7), whereas mice with a single knockout of APP gene family members are viable. However, single APP knockout mice show deficits in spatial learning and long-term potentiation, which can be rescued by a knockin allele of sAPP α (8). APP/APLP2 and APLP1/APLP2 double knockout mice demonstrate a reduced viability similar to the triple knockout model and the APP/APLP2 knockout mice suffer from defective neuromuscular synapses (9). Surprisingly, triple knockout neurons derived from triple knockout embryonic stem cells did not show macroscopic abnormalities (10). At the molecular level, a decreased expression of the vesicular glutamate transporter 2 was detected in glutamatergic neurons differentiated from APP/APLP2 knockout embryonic stem cells (11). In astrocytes from mice lacking APP, a deregulation of Ca²⁺ signaling was evident accompanied by a down-regulation of TRPC1 (C-type transient receptor potential) and Orai1 proteins, which are components of store-operated channels (SOCs). Taken together, our present knowledge of the APP and its family proteins is limited. Within this work, we have established an APP/APLP1/APLP2 cell culture knockdown model and studied changes in protein abundance by proteomics with subsequent functional studies. We demonstrate validated protein abundance changes for MAT2A and PRDX4 as well as changes in SAM concentrations, which is a product of MAT2A enzyme activity. Finally, we discovered effects on *BACE1* and *PSEN1* gene expression. Our results point to a pivotal role of the APP protein family in differential methylation. Our cell culture model is able to reflect AD related mechanisms in part. For example, the reduced level of the soluble amyloid precursor protein alpha is evident in our model as well as in AD (12). Additionally, recruitment of the adapter protein FE65 to the cell membrane was suggested to be diminished in AD (13), which is mimicked by the absence of the APP family intracellular domains in our model as well. Thus, our findings might be of interest for AD pathophysiology.

EXPERIMENTAL PROCEDURES

Cell Culture—The APP/APLP1/APLP2 knockdown was established by simultaneous transfection with GIPZ lentiviral shRNAir vectors (Open Biosystems, Huntsville, AL) in HEK293T cells. For the control state, a non silencing GIPZ lentiviral shRNAir vector (Open Biosystems) was used. First 180×10^4 cells were seeded on 10 cm cell culture dishes (TPP, Switzerland) using five dishes for control and five dishes for the knockdown condition ($n = 5$). Cells were cultivated at 37 °C and 5% CO₂ in 10 ml minimum essential medium (MEM) (Sigma-Aldrich) supplemented with 1% Penicillin/Streptomycin (PS) and 10% fetal calf serum (Invitrogen, Carlsberg CA). 48h after seeding HEK293T cells were transfected using lipofectamine reagent METAFECTENE™ (Biontex, Germany). For each cell culture dish 36 μ l METAFECTENE™ and 36 μ g total DNA was used whereby 5 ml MEM was removed before transfection. The transfection procedure was done according to the manufacturer's instructions. The hairpin sequences of the applied GIPZ lentiviral shRNAir vectors are shown in Table I. To improve transfection efficiency, puromycin was used to get rid of untransfected cells. Twenty-four hours after transfection the final MEM dish volume was adjusted to 7 ml total MEM and 12 μ g/ml puromycin was added in each cell culture dish. Cells were selected for 96 h with puromycin following by MEM filtration through a Filtropur S 0.2 sterile filter (Sarstedt, Germany). The filtered MEM was added again to the selected cells. Twelve hours after filtration procedure cells were washed with 7 ml cold (4 °C) GIBCO™ Phosphate buffered saline +/+ (PBS +/+) (Invitrogen) and harvested with 8 ml cold PBS +/+. 2 ml were used for RNA and 6 ml for protein isolation. Subsequently PBS +/+ (Invitrogen) was removed by centrifugation at 200rcf at 4 °C. To ensure a sufficient protein and RNA amount after cell harvesting, the complete cell culture procedure was repeated and the resulting cell pellets were combined. For protein isolation, cell pellets were sonicated in DIGE buffer (7 m Urea, 2 m Thiourea, 2% 3-[(3-cholamidopropyl)dimethylammonio]propanesulfonate, 130 mm dithiothreitol, 30 mm Tris-HCl, pH8.5) and the cellular extracts were centrifuged at 15.500 rcf for 15 min at 4 °C. The supernatants were used for subsequent experiments and the protein concentration was determined by amino acid analysis (ASA) on a HPLC Alliance 2695 instrument (Waters, Milford, MA).

Quantitative PCR (qPCR)—To quantify mRNA levels of APP/APLP1/APLP2, SYBR Green real-time PCR assays were performed on a RotorGene RG-3000 device (Corbett Life Science, Sydney, Australia). RNA lysates from cell culture were gained using the NucleoSpin RNA II kit (Machery Nagel, Germany) according to the manufacturer's protocol. Template cDNA was synthesized from 2 μ g total RNA using the RevertAid™ First Strand cDNA Synthesis Kit (Thermo Scientific) and random hexamer primers following manufacturer's instructions. Cycling conditions were 95 °C for 15min, followed by 45 cycles of 95 °C for 15 s, 56 °C for 30 s, and 72 °C for 30 s. The dCt values were calculated using GAPDH as control. Experiments were performed in triplicate for each clone analyzed. Melting curve analysis confirmed that only one product was amplified. For statistical analysis of all quantitative PCR experiments, normal distribution of data was assured and remaining gene expression was calculated by the method of Livak and Schmittgen (14). For quantification of mRNA levels of MAT2A, PDRX4, PSEN1, and BACE1, the same qPCR procedure was used. All sense and antisense primer sequences used in qPCR experiments are given in Table II.

Immunoblotting/Immunofluorescence—Total protein was separated by SDS-PAGE using 4–12% NuPAGE™ Bis-Tris gels (Invitrogen) and proteins were transferred to nitrocellulose. The Odyssey Infrared Imaging System (LI-COR Biosciences, Lincoln, NE) was used for protein detection. The APP blot was probed with a self made anti human full length APP antibody (see Acknowledgment). For the APP blot, 25 μ g total protein was used for each lane and an antibody

TABLE I
GIPZ lentiviral shRNAir vectors (Open Biosystems, USA)

shRNAir	Hairpin sequence	Catalog no.	Clone id
APP (used for main experiment)	TGCTGTTGACAGTGAGCGCGGTGCTCCATTATAGAAATAAGTGAAGCC ACAGATGTATTATCTATAAGACCGATGCTACTGCTCGGGA	RHS4430-98713590	V2LHS_231737
APP (used for OFF-TARGET preclusion)	TGCTGTTGACAGTGAGCGGTGCTCCATTATAGAAATAAGTGAAGCC CAGATGTAATATTGCTGTTGACAGTGAGCGCGGTGCTCCATTATAG AATAAGTGAAGCCATAATAGACCGTGCCTACTGCTCGGA	RHS4430-98715779	V2LHS_233086
APLP1 (used for main experiment)	TGCTGTTGACAGTGAGCGGTGCTCCATTATAGAAATAAGTGAAGCC CAGATGTAATATTGCTGTTGACAGTGAGCGCGGTGCTCCATTATAG AATAAGTGAAGCCATAATAGACCGTGCCTACTGCTCGGA	RHS4430-98850747	V2LHS_48899
APLP1 (used for OFF-TARGET preclusion)	TGCTGTTGACAGTGAGCGGTGCTCCATTATAGAAATAAGTGAAGCC AGATGTAATATTGCTGTTGACAGTGAGCGCGGTGCTCCATTATAG AATAAGTGAAGCCATAATAGACCGTGCCTACTGCTCGGA	RHS4430-98487326	V2LHS_48896
APLP2 (used for main experiment)	TGCTGTTGACAGTGAGCGGTGCTCCATTATAGAAATAAGTGAAGCC CAGATGTAATATTGCTGTTGACAGTGAGCGCGGTGCTCCATTATAG AATAAGTGAAGCCATAATAGACCGTGCCTACTGCTCGGA	RHS4430-98895684	V2LHS_132589
APLP2 (used for OFF-TARGET preclusion)	TGCTGTTGACAGTGAGCGGTGCTCCATTATAGAAATAAGTGAAGCC CAGATGTAATATTGCTGTTGACAGTGAGCGCGGTGCTCCATTATAG AATAAGTGAAGCCATAATAGACCGTGCCTACTGCTCGGA	RHS4430-98476146	V2LHS_132591
Non-silencing-control	Not specified by manufacturer	RHS4346	/

dilution of 1:100 in StartingBlock™ TBS Blocking Buffer (Thermo Scientific) was applied. The APLP2 blot was probed with a full length APLP2 antibody (Cat no: 171617; Calbiochem, San Diego, CA) using a dilution of 1:500 in StartingBlock™ TBS Blocking Buffer and 25 µg total protein. The MAT2A blot was probed with a MAT2A antibody (dilution factor 1:1000, 15 µg total protein, Cat no: ab77471; Abcam, Cambridge, UK). The PRDX4 blot was probed with a PRDX4 antibody (dilution factor 1:1000 in StartingBlock™ TBS Blocking Buffer, 25 µg total protein, Cat no: ab59542; Abcam). Additionally, all immunoblots were incubated with a β-actin antibody (dilution factor 1:10000, Cat no: A1978; Sigma Aldrich, Germany). The β-actin signal intensity was used for normalization. Secondary antibodies were used as follows: IRDye™ 800CW antibody (dilution factor 1:15000, Cat no: 926-32211; LI-COR Biosciences). IRDye™ 680CW antibody (dilution factor 1:15000, Cat no: 926-32220; LI-COR Biosciences). Densitometric quantification was carried out with Odyssey Application Software version 3.0.21 (LI-COR Biosciences).

For immunofluorescence experiments, HEK293T cells were washed with PBS +/+, fixed with standard 4% paraformaldehyde, permeabilized with standard 0.5% Triton X-100 and incubated with the corresponding antibody as follows: MAT2A antibody (dilution factor 1:50, Cat no: ab77471; Abcam); PRDX4 antibody (dilution factor 1:50, Cat no: ab59542; Abcam); secondary TRITC antibody (dilution factor 1:200, Cat no: T5268; Sigma-Aldrich); nuclear visualization was carried out with Hoechst Staining. Images were obtained using the fluorescence microscope IX51 (Olympus Microscopy, UK).

Mass Spectrometry—A label-free approach based on spectral counts was used for relative quantification of protein abundance in knockdown versus control cells. The method was established in our lab and has been successfully used within other projects (15, 16). In brief, total cell lysates (20 µg each lane) were separated by SDS-PAGE with 4–12% NuPAGE™ Bis-Tris Gel (Invitrogen) and stained with Imperial™ Protein Stain (Thermo Scientific). Following destaining, the complete gel was reduced using dithiothreitol and alkylated with iodoacetamid. The gel was cut into ten horizontal slices and afterward every lane was cut in ten pieces (compare Fig. 2A). In-gel digestion was performed overnight at 37 °C with trypsin (Promega, Madison, WI) in 10 mM HCl and 50 mM ammonium hydrogen carbonate (NH₄HCO₃) at pH 7.8. Resulting peptides were extracted once with 100 µl of 1% formic acid (FA), and twice with 100 µl of 5% FA, 50% ACN (acetonitrile). Extracts were combined and ACN was removed *in vacuo*. For LC-MS analysis, a final volume of 40 µl was prepared by addition of 1% FA.

Electrospray tandem mass spectrometry (ESI-MS/MS) was performed on a HCT Plus ion trap instrument (Bruker Daltonics, Billerica, MA) equipped with a nanoelectrospray ion source (Bruker Daltonics) using distal coated SilicaTips Pico (FS360-20-10-d-20, Coating: 1P-4P; New Objective) coupled to an UltiMate 3000 LC system (Dionex, Germany). After washing, the trap column was serially connected with an analytical C18 column (Dionex, 75 µm × 15 cm, particle size 2 µm, pore size 100 Å). The peptides were separated with a flow rate of 300 nl/min using the following solvent system: (A) 0.1% FA; (B) 84% ACN, 0.1% FA. In a first step, a gradient from 5% B to 35% B (100 min) was used, followed by an elution step at 95% B for 5 min and a finally equilibration step at 5% B for 25 min.

Fragment ions were generated by low-energy collision-induced dissociation (CID) on isolated ions with a fragmentation amplitude of 0.5 V. MS spectra were summed from four individual scans ranging from *m/z* 300–1500 with a scanning speed of 8.100 (*m/z*)/s. MS/MS spectra were a sum of two scans ranging from *m/z* 100–2800 at a scan rate of 26.000 (*m/z*)/s.

The data associated with this manuscript may be downloaded from the ProteomeCommons.org Tranche network using the following hash:

TABLE II
Primer Sequences for quantitative PCR (5'–3' orientation)

mRNA	Sense primer	Antisense primer
APP	5'-TGGCCAACATGATTAGTGAACC-3'	5'-AAGATGGCATGAGAGCATCGT-3'
APLP1	5'-CACCAGTTGTGCCCTTCC-3'	5'-GGCCTCACTCACAAATTCACC-3'
APLP2	5'-CGACGGCACCATGTCAGAC-3'	5'-CAACGAGGCATCACGGC-3'
MAT2A	5'-CTTCCGCACACCGACACCAACAT-3'	5'-TCGATGAACGCCTCGTGGGAAGC-3'
PRDX4	5'-CGTGTCTGCGCTCGCGTG-3'	5'-GGCCGTGGTCCGGAGTTGTC-3'
PSEN1	5'-GCGGCGGGGAAGCGTATACC-3'	5'-GGCCAAGCTGTCTAAGGACCGC-3'
BACE1	5'-GGGCTGGCCTATGCTGAGATTGC-3'	5'-GCACCACAAAGCTGCAGGGAGAA-3'
GAPDH	5'-GCCACATCGCTCAGACACC-3'	5'-AATCCGTTGACTCCGACCTTC-3'

JwwDuyx9JLhaPKdQA8w+GmMiiRmw2qPaxNwDpITehfy7zRkZ+u0
hVRiCHEN+qbtJLKlbiZUJFMJSSRV0Xs5SeLIGFZoAAAAAAA5zw==.

The hash may be used to prove exactly what files were published as part of this manuscript's dataset, and the hash may also be used to check that the data has not changed since publication.

Data Processing and Database Search—Raw files were transformed to *.mgf-files (Data Analysis 4.0, Bruker Daltonics), imported in ProteinScape™ (version 2.1, Bruker Daltonics), and analyzed using Mascot (Matrixscience, UK) with a peptide mass tolerance of 1.2 Da and a fragment mass tolerance of 0.3 Da. Searches were performed allowing one missed cleavage site after tryptic digestion. Carbamidomethylation (C), oxidation (M), and phosphorylation (S,T,Y) were considered as variable modifications. All data were searched against a database created by DecoyDatabaseBuilder (17) containing the whole UniProt/Swissprot (release 2011/06, 529056 entries) with one additional shuffled decoy for each protein, resulting in a database containing 1.058.112 entries.

Protein Quantification and Pathway Analysis—After peptide identification an algorithm that uses a given minimal peptide score (minPepScore) and a minimal number of peptides per protein (minNrPeps) was applied. The algorithm performs the following steps:

Score calculation for all proteins by adding up the Mascot ion scores of the protein's peptides, which have a score of at least minPepScore. Here, a peptide is defined by an amino acid sequence and its modifications. If two peptides are equal except for the score, only the higher score is taken. Reporting the highest scoring protein group (a group consists of all proteins in the database containing the same set of identified peptides), which has at least minNrPeps peptides not yet flagged as used up and flag all the peptides of the reported proteins as used up. Repetition of step 2 until no more protein groups get reported.

A local false discovery rate (FDR) was calculated for each protein group, regarding a group as decoy, if it consists of decoy proteins only. With this strategy the minPepScore was calculated, which yielded the list with the most target (opposed to decoy) groups beneath an FDR-threshold of 5%. For the given data a minNrPeps of 2 was used to exclude "one hit wonders," which yielded a minPepScore of 22 for the longest list. Among the proteins in this list, every peptide spectrum match (PSM) was extracted.

These PSMs were further processed using the Pivot table function of Microsoft Excel resulting in a table representing spectral counts for every peptide belonging to a certain protein. Processed spectral counts (PSC) based on spectral and peptide counts were calculated as described previously (16, 18) and subsequently used as basis for label-free quantification. In brief, PSC calculation was performed by summing up all spectral counts belonging to the respective protein. To identify differentially expressed proteins, the ratio between the averaged spectral indices of the knockdown samples and controls was calculated and Student's *t* test was conducted for each protein. In order to control the FDR, the resulting *p* values were adjusted for multiple testing according to Benjamini and Hochberg (19). However, adjusted *p* value calculation

was inappropriate for our approach as the number of identified proteins (which is a determining factor for the correction calculation) is extremely large in our study caused by the use of a sensitive MS instrument. Thus, all proteins reported to be relevant in this work have been validated by independent methods. Initially, a significant *t* test (<0.05) and a spectral index ratio > 1.7 was used to assign a protein as potential candidate for subsequent experiments. The complete protein and peptide data are given in the supplement file MS_data.xlsx.

The pathway analysis was done with two independent software, IPA 9.0 (Ingenuity Pathway Analysis, Ingenuity Systems, USA, <http://www.ingenuity.com>) and STRING 9.0 (Search Tool for the Retrieval of Interacting Genes/Proteins, EMBL Institute, Europe, <http://string-db.org>) according to our experience of pathway tools in proteomics (18).

SAM-assay—S-adenosylmethionine (SAM) levels were measured with Bridge-It™ S-adenosylmethionine Fluorescence Assay (Mediomics, St. Louis, MO, USA) using a 384-well microplate format. At first a SAM standard curve was recorded from 0.195 μmol to 100 μmol with the Infinite™ 200 PRO device (Tecan Group, Männedorf, Switzerland) according to manufacturer's protocol and plotted with a Boltzmann sigmoidal fit. Afterward, SAM levels were quantified in control and knockdown samples at 25 °C with adjusted excitation at 485 nm and emission at 665 nm.

Human Frontal Cortex Brain Samples—All human post-mortem frontal cortex samples were collected from the Center for Neuropathology and Prion Research, Ludwig Maximilians University Munich. Prior to autopsies, we obtained agreement from patient's families to use samples for research. The neuropathological diagnosis of AD was made according to established criteria (20, 21). The control group consisted of brains from cases without neurological and neuropathological abnormalities. Protein lysates were obtained from frozen post-mortem samples of the frontal gray matter of nine individuals with AD and 13 individuals of age matched controls. Immunoblotting analysis with subsequent densitometry was done as described above. An ethical vote for the work with human brain tissue is available (register No. 2875, ethical commission of the Ruhr-University Bochum).

RESULTS

Knockdown of APP, APLP1, and APLP2 in HEK293T Cells—To gain further insights in the physiological role of the APP family and the possible consequences for AD, we established a triple APP/APLP1/APLP2 knockdown cell culture model (simultaneously termed knockdown). We used HEK293T cells, which express all three APP family members. Real-time PCR (qPCR) analysis of *APP*, *APLP1*, and *APLP2* using *GAPDH* as house-keeping control revealed highest expression of *APP* in HEK293T cells (*Ct* = 19.17, Fig. 1A).

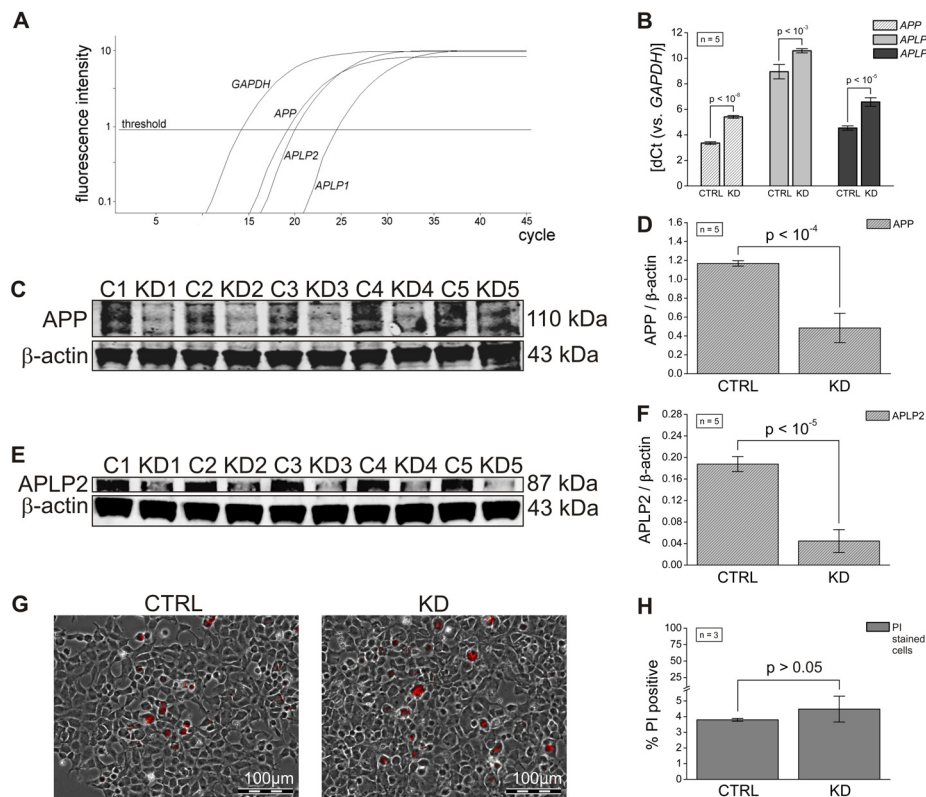


FIG. 1. Generation of an APP/APLP1/APLP2 cell culture knockdown model. A, HEK293T cells demonstrate simultaneous expression of all three members of the APP family. Using *GAPDH* as control and an intensity threshold of 0.09, expression level of *APP* was the most prominent ($C_t = 19.17$), followed by *APLP2* ($C_t = 19.98$). *APLP1* expression levels was moderate ($C_t = 24.46$). B, Using shRNA constructs for *APP*, *APLP1*, and *APLP2* a significant knockdown of all APP family members was achieved after 4.5 days selection with puromycin (*APP* $p < 10^{-8}$, *APLP1* $p < 10^{-3}$, *APLP2* $p < 10^{-5}$; higher dCt values correspond to lower RNA levels in comparison to the control). Significance was calculated using the dCt values, which are illustrated in the Figure. Knockdown efficiency (not shown in the Figure) was calculated as published by the method of Livak and Schmittgen (16). *APP* levels were silenced to 24.9% (+0.9%, -0.8%), *APLP1* to 32.1% (+1.7%, -1.6%) and *APLP2* to 24.3% (+2.7%, -2.4%) remaining gene expression. Random shRNA constructs were used to establish control samples in a similar fashion. In total, 5 knockdown and 5 control samples were established. C, The knockdown of *APP* was also evident at the protein level. D, Densitometry using β -actin as control revealed a significant silencing ($p < 10^{-4}$) for all 5 samples versus 5 controls. E, Similarly, the knockdown of *APLP2* was evident at the protein level ($p < 10^{-5}$, according to densitometry, $n = 5$). F, Immunoblotting analysis of *APLP1* failed putatively as a result of poor antibody quality and low abundance of *APLP1* in the cells (compare A)). G, Propidium iodide staining of knockdown and control cells revealed no significant changes (H) not pointing to elevated apoptosis/cell death.

APLP2 was moderately expressed in the cells ($C_t = 19.98$), whereas *APLP1* revealed lowest expression level within the APP family ($C_t = 24.46$). Initial experiments using siRNA as well as shRNA for a significant and fundamental knockdown of all members failed putatively as a result of poor interfering RNA quality (data not shown). However, a significant and prominent knockdown was achieved using selectable shRNA constructs after application of puromycin for 4.5 days. As a control, we established a cell line transfected with random shRNA constructs, which were selected for the same time as well. In total, five knockdown clones and five controls were used for subsequent experiments. Quantification of knockdown levels was performed by qPCR and immunoblotting. The qPCR analysis demonstrated a significant knockdown of *APP* ($p < 10^{-8}$, Fig. 1B, higher dCt values correspond to lower RNA levels in comparison to the control)

with a calculated remaining gene expression of 24.9% (+0.9%, -0.8%). In addition, also the knockdown of *APLP1* was significant ($p < 10^{-3}$, Fig. 1B) as was that of *APLP2* ($p < 10^{-5}$, Fig. 1B). The calculated remaining gene expression of *APLP1* was 32.1% (+1.7%, -1.6%) and of *APLP2* 24.3% (+2.7%, -2.4%). Significance of *APP* and *APLP2* reduction in knockdown cells could also be confirmed at the protein level. Immunoblotting of *APLP1* failed probably as a result of poor antibody quality. Moreover, in the HEK293T cells *APLP1* is the protein with lowest gene expression level among the APP family (compare Fig. 1A) potentially hampering the protein detection. However, protein levels of *APP* could be significantly silenced ($p < 10^{-4}$, β -actin signal intensity was used for normalization (Fig. 1C) with densitometric analysis in Fig. 1D). In analogy, knockdown of *APLP2* was also significant at the protein level ($p < 10^{-5}$, Figs. 1E,

1F). Herms et al. showed that a knockdown of all APP family members results in a lethal phenotype (7). To investigate putative toxicity of the family knockdown in HEK293T cells, we stained the cells (knockdown versus control) with propidium iodide (PI) (Fig. 1G) and counted PI positive cells as percentage of total cells. No significant changes could be observed (Fig. 1H). Taken together, a cell culture model with a triple simultaneous knockdown of APP, APLP1, and APLP2 was established, which was subsequently used for the analysis of protein abundances versus controls.

Knockdown of the APP Family Leads to Prominent Proteome Changes—For the differential proteome analysis, we used a newly established workflow based on 1D-gel pre-fractionation of total cell lysates, tryptic digestion, and HCT MS label-free analysis (Fig. 2A). Quantification was performed according to a label-free procedure on the basis of processed spectral counts, which was already successfully used for other studies in our group (16, 18). In our study, we compared five biological replicates of the APP family knockdown versus five biological replicate controls revealing 34 proteins with significant abundance changes. In total, 2075 proteins were identified and relatively quantified using standard criteria of the label-free approach (compare Experimental Procedures). Among the total identified proteins, 29 correspond to the so called black-and-white list that are proteins identified only in one group with at least three measured values. The complete results are given in Table III. Interpretation of the results and choice of candidates for subsequent validation experiments was derived from a triplex strategy: first, we evaluated the significance of the results from the label-free study (statistical significance, ratio of abundance changes). Second, protein candidate selection was done with the help of the pathway analysis software IPA 9.0 (Ingenuity Pathway Analysis) and STRING 9.0 (Search Tool for the Retrieval of Interacting Genes/Proteins). Therefore all proteins shown in Table III were uploaded in the software tools. Affected networks, canonical pathways, protein family and protein localization were assessed according to our experience with pathway tools (24). Finally, recent literature findings in respect to APP signaling and AD were manually assessed and aligned with the pathway results. Data upload in the mentioned software tools resulted in the pathway cartoons that are given in Fig. 2B (IPA) and Fig. 2C (STRING), respectively. Differences in pathway generation resulted from different analysis strategies in IPA and STRING. IPA generates networks including proteins of the uploaded list in addition to further proteins that are important for the pathway. In contrast, STRING generates networks just from the complete protein list given (the pathway presented by STRING can also be adapted by the use of the more or less function). In IPA, we selected one network as the most relevant (Fig. 2B), that contained most of the proteins identified to be differential in abundance between the APP/APLP1/APLP2 knockdown cells versus

controls. Within this network, IPA identified “Apoptosis Signaling” as the most prominent canonical pathway including eight proteins, namely apoptotic chromatin condensation inducer in the nucleus (ACIN1), BCL-2-associated X protein (BAX), Caspase, extracellular signal-regulated protein kinase 1/2 (ERK1/2), c-Jun-N-terminal kinase (JNK), nuclear factor kappa-light-chain-enhancer of activated B cells (NF κ B), p38 mitogen-activated protein kinases (p38 MAPK), and poly (ADP-ribose) polymerase 1 (PARP1). Interestingly, the enzyme methionine adenosyltransferase II, alpha (MAT2A) was recently identified to bind PARP1 (22) and its product SAM was already described to have a pivotal role in AD (23). Additionally, peroxiredoxin 4 (PRDX4) emerged to be a promising candidate as proteins of the PRDX family are known to be regulated in brain tissue of AD patients versus controls (24). Moreover, MAT2A as well as PRDX4 turned out to belong to the most significant results of our proteome analysis (compare Table III, $p < 0.005$ for both proteins). Finally, the decision not to select the apoptosis relevant proteins for validation was done based on our first experiments that did not demonstrate significant changes in the PI staining of knockdown cells versus controls (Figs. 1G, 1H). Additionally, based on our experience in label-free proteomics, proteins in the knockdown and in the control samples (indicated by *** in Figs. 2B, 2C (as true for MAT2A and PRDX4)) correspond to highest quality results.

To get a “second opinion,” we assessed the data analysis by the alternative pathway software STRING that combines all identified differentially abundant proteins in one network as shown in Fig. 2C. Results outlined different nodes of action within the differentially abundant proteins. Similar to the IPA analysis proteins involved in apoptosis were highlighted (BAX, PARP1, BCL-2-associated transcription factor 1 (BCLAF1), B-cell receptor-associated protein 31 (BCAP31)). Additionally, the ribosomal proteins RPS23, RPLP0, and RPN1 form an interaction network, where RPN1 was identified as an ubiquitin-like protein binding subunit. Applying the criteria mentioned above, we selected the differentially (APP/APLP1/APLP2 knockdown versus control) abundant proteins MAT2A and PRDX4 for subsequent experiments.

Validation of MAT2A and PRDX4 as APP Family Dependent Regulated Proteins—Using standard immunoblotting technique, we next aimed to validate our findings for MAT2A, which was found to be lower abundant in the knockdown cells using the label-free approach. Indeed, we were able to identify a fundamental down-regulation of MAT2A in the knockdown cells (Fig. 3A). Densitometry revealed the significance of our findings ($p < 10^{-5}$, Fig. 3B). MAT2A protein abundance changes caused by the lack of APP family members might be the result of the activity of the different domains of the protein, especially sAPP and AICD (sAPLP’s and APLPICD’s). The latter was suggested to act as a transcriptional regulator. To gain further insights in a putative regulation of MAT2A mRNA levels by AICD, we next assessed MAT2A gene

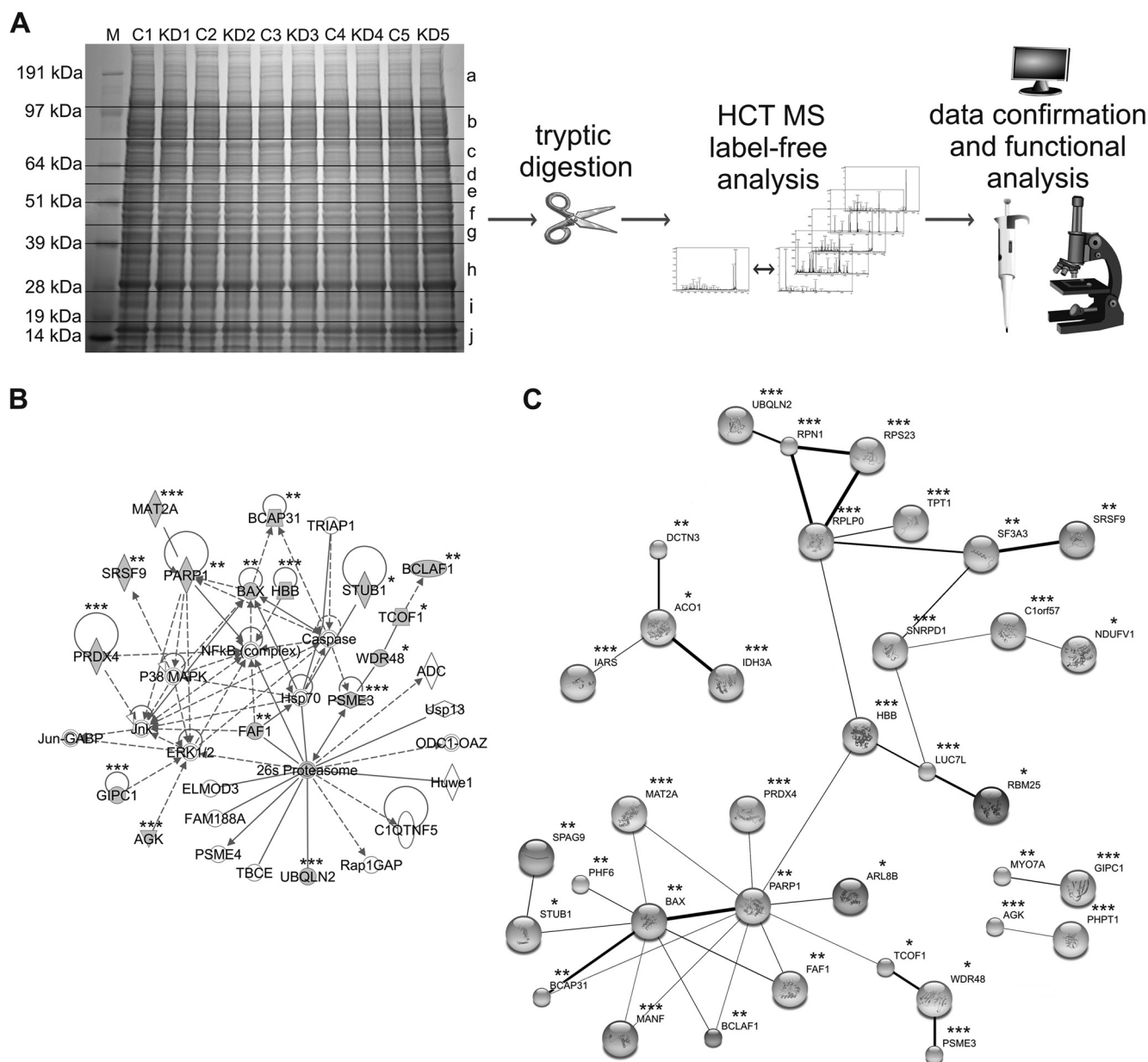


FIG. 2. Application of label-free proteomics for the identification of differentially abundant proteins between APP/APLP1/APLP2 knockdown cells versus controls. A, A newly established label-free workflow including 1D-gel pre-fractionation, tryptic digestion, HCT mass spectrometry (MS) label-free analysis, and processed Spectral Index Analysis was applied to examine protein abundance changes in total protein lysates from five knockdown (KD) cells versus 5 controls (C), M Δ Protein Ladder. B, Pathway analysis using the commercial software IPA revealed changes in apoptosis signaling, which was further confirmed by the analysis using the software tool STRING. C, The regulated proteins are divided in highly significant findings (*** Δ found in CTRL and KD) corresponding to the standard data analysis procedure (compare Experimental Procedures) and so called black-and-white proteins (* Δ only found in CTRL, ** Δ only KD), which were measured in just one sample group. Proteins without an asterisk were added by the software. Notably, both software tools reported a recent association of PARP1 to MAT2A and PRDX4, whose enzymatic product is known to play a role in AD for a long time.

expression in the knockdown cells versus controls using qPCR. Notably, a significant reduction in MAT2A gene expression was also evident at the mRNA level ($p < 10^{-8}$, Fig. 3C). To study the subcellular localization of the MAT2A protein, we next stained fixed APP/APLP1/APLP2 knockdown and control cells using immunofluorescence (Fig. 3D).

MAT2A was predominantly localized in the nucleus and perinuclear in small aggregates, as clearly shown by HOECHST nuclear counterstain. Additionally, a weaker signal was observed in the cytosol. Subcellular localization was the same in knockdown as well as in control cells pointing to a function of MAT2A in the mentioned compart-

TABLE III
Results of the label-free study

APP/APLP1/APLP2 knockdown (KD) vs. control (CTRL.), five biological replicates of kd and ctrl. were compared. PSC* = processed spectral counts (for more information see part Experimental Procedures), reg. direction** up = up-regulation corresponds to higher abundance in APP/APLP1/APLP2 knockdown cells, reg. direction** down = down-regulation corresponds to lower abundance in APP/APLP1/APLP2 knockdown cells, gel slice*** according to sample pre-fractionation (compare Figure 2A, for more information see part Experimental Procedures), na. = not applicable.

	Accession	CTRL. PSC*	KD PSC*	Change fold	p value	Reg. direction**	Gel slice***
Protein (found in CTRL. & KD)							
CCDC56 (Coiled-coil domain-containing protein 56)	IPI00022277	0.60	2.80	4.68	0.0005	up	j
PHPT1 (Phosphohistidine phosphatase 1)	IPI00299977	3.03	0.73	4.15	0.0006	down	j
UBQLN2 (Ubiquilin-2)	IPI00409659	2.81	0.60	4.69	0.0010	down	d
PRDX4 (Peroxiredoxin-4)	IPI00011937	7.82	3.39	2.31	0.0011	down	h, i
XTP3TPA (XTP3-transactivated gene A protein)	IPI00012197	1.62	0.19	8.47	0.0021	down	i
DBNL (Drebrin-like protein)	IPI00456925	0.18	0.99	5.41	0.0031	up	e
VPS26B (Vacuolar protein sorting-associated protein 26B)	IPI00059264	0.43	2.02	4.70	0.0038	up	g
MAT2A (S-adenosylmethionine synthetase isoform type-2)	IPI00010157	7.68	1.69	4.54	0.0047	down	f
ATP6V1G1 (Vacuolar proton pump subunit G 1)	IPI00025285	1.89	0.54	3.47	0.0052	down	j
MANF (Mesencephalic astrocyte-derived neurotrophic factor)	IPI00924819	2.60	0.78	3.32	0.0071	down	i
PSME3 (Proteasome activator complex subunit 3)	IPI00030243	3.90	1.94	2.01	0.0103	down	h
RPS23 (40S ribosomal protein S23)	IPI00218606	1.89	3.72	1.97	0.0113	up	i, j
HSPC152 (TRM112-like protein)	IPI00009010	0.36	2.37	6.65	0.0139	up	j
RPN1 (Dolichyl-diphosphooligosaccharide-protein glycosyltransferase)	IPI00025874	3.55	8.68	2.45	0.0171	up	a, b, d
HBB (Truncated beta-globin)	IPI00815947	1.04	2.73	2.61	0.0177	up	j
SFXN1 (Sideroflexin-1)	IPI00009368	7.74	3.70	2.10	0.0203	down	h
TPT1 (Translationally-controlled tumor protein)	IPI00550900	1.14	3.17	2.78	0.0214	up	i
ABCF1 (ATP-binding cassette sub-family F member 1)	IPI00873899	1.39	3.51	2.52	0.0228	up	b
LUC7L (Putative RNA-binding protein Luc7-like 1)	IPI00793246	1.88	4.22	2.24	0.0241	up	f, g
RANBP2 (E3 SUMO-protein ligase RanBP2)	IPI00221325	0.20	1.83	9.07	0.0253	up	a
AGK (Acylglycerol kinase, mitochondrial)	IPI00019353	2.04	0.38	5.42	0.0276	down	f
IDH3A (Isocitrate dehydrogenase 3 [NAD+] alpha)	IPI00030702	3.30	1.52	2.17	0.0304	down	g, h
RPLP0 (RPLP0 18 kDa protein)	IPI00791188	0.19	1.82	9.48	0.0310	up	g, h, i
THUMPDI (THUMP domain-containing protein 1)	IPI00550243	1.65	0.55	2.99	0.0316	down	f
COPS8 (COP9 signalosome complex subunit 8)	IPI00009480	2.76	1.19	2.33	0.0316	down	i
SNRPD1 (Small nuclear ribonucleoprotein Sm D1)	IPI00647160	0.36	1.28	3.59	0.0350	up	j
SKIV2L2 (Superkiller viralicidal activity 2-like 2)	IPI00647217	2.05	0.56	3.64	0.0366	down	b
CACYBP (Calcyclin-binding protein)	IPI00395627	2.51	6.74	2.69	0.0424	up	h
ACIN1 (Apoptotic chromatin condensation inducer in the nucleus)	IPI00215975	5.05	2.76	1.83	0.0435	down	a, b, c
C1orf57 (Nucleoside triphosphate phosphohydrolase)	IPI00031570	3.32	1.39	2.39	0.0450	down	i
DNAJC19 (DnaJ (Hsp40) homolog, subfamily C, member 19)	IPI00795263	1.40	0.13	11.03	0.0462	down	j
GIPC1 (PDZ domain-containing protein GIPC1 isoform 2)	IPI00401971	0.19	1.34	7.03	0.0466	up	g
PRPSAP2 (Phosphoribosyl pyrophosphate synthetase-associated protein 2)	IPI00796213	2.31	0.74	3.11	0.0489	down	g
IARS (Isoleucyl-tRNA synthetase, cytoplasmic)	IPI00644127	8.94	15.86	1.77	0.0496	up	a
Protein (only found in CTRL.)							
ACO1 (Iron-responsive element-binding protein 1)	IPI00008485	1.23	0.00	na.	na.	na.	b
BZW2 (Basic leucine zipper and W2 domain-containing protein 2)	IPI00022305	0.62	0.00	na.	na.	na.	f
TSFM (Elongation factor Ts, mitochondrial)	IPI00021016	0.63	0.00	na.	na.	na.	h
ARL8B (ADP-ribosylation factor-like protein 8B)	IPI00940959	0.60	0.00	na.	na.	na.	i
DDX18 (ATP-dependent RNA helicase DDX18)	IPI00301323	1.51	0.00	na.	na.	na.	c
FUSIP1 (FUS-interacting serine-arginine-rich protein 1)	IPI00645384	0.59	0.00	na.	na.	na.	g, i
HP1BP3 (Heterochromatin protein 1, binding protein 3)	IPI00878947	0.78	0.00	na.	na.	na.	c
MARCKSL1 (MARCKS-related protein)	IPI00641181	1.40	0.00	na.	na.	na.	g, h
NDUFV1 (NADH dehydrogenase flavoprotein 1)	IPI00221298	1.38	0.00	na.	na.	na.	e, f
PSME2 (Proteasome activator subunit 2)	IPI00746205	0.63	0.00	na.	na.	na.	h
RBM25 (RNA-binding protein 25)	IPI00925670	0.80	0.00	na.	na.	na.	b
STUB1 (STIP1 homology and U box-containing protein 1)	IPI00645380	0.59	0.00	na.	na.	na.	h
SYNJ2BP (Synaptojanin-2-binding protein)	IPI00299193	0.73	0.00	na.	na.	na.	j
TCOF1 (Treacle protein)	IPI00815731	1.35	0.00	na.	na.	na.	a
WDR12 (WD repeat-containing protein 12)	IPI00304232	0.63	0.00	na.	na.	na.	e, f
WDR48 (WD repeat-containing protein 48)	IPI00792902	0.62	0.00	na.	na.	na.	c
Protein (only found in KD)							
BAX (Isoform Epsilon of Apoptosis regulator BAX)	IPI00071059	0.00	0.61	na.	na.	na.	i

TABLE III—continued

	Accession	CTRL. PSC*	KD PSC*	Change fold	p value	Reg. direction**	Gel slice***
BCAP31 (B-cell receptor-associated protein 31)	IPI00218200	0.00	0.73	na.	na.	na.	a, b, h
BCLAF1 (Bcl-2-associated transcription factor 1)	IPI00413673	0.00	0.80	na.	na.	na.	a, b
CCT8 (CCT8 chaperonin containing TCP1, subunit 8)	IPI00302925	0.00	0.58	na.	na.	na.	d, e
SF3A3 (Splicing factor 3A subunit 3)	IPI00029764	0.00	1.00	na.	na.	na.	d, e
CNOT10 (CCR4-NOT transcription complex subunit 10)	IPI00926913	0.00	0.61	na.	na.	na.	c
DCTN3 (Dynactin subunit 3)	IPI00747408	0.00	0.80	na.	na.	na.	i
FAF1 (FAS-associated factor 1)	IPI00070643	0.00	0.63	na.	na.	na.	c
MYO7A (Myosin VIIA)	IPI00943793	0.00	0.44	na.	na.	na.	a
PARP1 (Poly ADP-ribose polymerase 1)	IPI00449049	0.00	1.36	na.	na.	na.	a, b, c, d, e, g
PHF6 (PHD finger protein 6)	IPI00397700	0.00	0.59	na.	na.	na.	f
SFRS9 (Splicing factor, arginine/serine-rich 9)	IPI00012340	0.00	0.78	na.	na.	na.	h
SPAG9 (C-jun-amino-terminal kinase-interacting protein 4)	IPI00744288	0.00	0.44	na.	na.	na.	a, i, j

ments. Images were taken to demonstrate subcellular localization and not for relative quantification. MAT2A is responsible for the synthesis of S-adenosylmethionine, which is a common co-substrate involved in methyl group transfer for a variety of different biomolecules. The cellular localization of MAT2A in the nucleus and perinuclear points to a role of SAM production/methylation presumably on biomolecules present in the mentioned compartments, especially DNA and proteins. Generation of methyl donors is highly important for the cell with the result that the MAT2A staining in many cellular compartments is reasonable.

In a similar fashion, we were able to validate our findings of different PRDX4 protein abundance using immunoblotting (Fig. 3E). Subsequent densitometry using β -actin as reference demonstrated significant PRDX4 down-regulation ($p < 0.05$, Fig. 3F). In contrast to MAT2A, qPCR analysis did not show differential gene expression for PRDX4 ($p > 0.05$, Fig. 3G). Immunofluorescence staining putatively demonstrated localization of PRDX4 in the ER, whereas changes between knockdown cells and controls were not evident (Fig. 3H). In analogy to the MAT2A staining, we did not address the intensity of the immunofluorescence staining. Taken together, we were able to validate the APP/APLP1/APLP2 dependent significant down-regulation of MAT2A and PRDX4 versus controls. MAT2A mRNA levels were significantly diminished, as well.

APP Family Dependent Down-regulation of MAT2A Results in an Increase of SAM—Several reports demonstrated quantitative differences of SAM, which is the product of an enzymatic reaction catalyzed by MAT2A, in samples from AD patients versus controls (23, 25–28). Encouraged by those findings, we next aimed to study SAM levels in our knockdown cells versus controls to uncover a putatively functional association of APP signaling and SAM generation. Therefore, we used a commercially available detection kit for SAM (see Experimental Procedures). Initially, we checked the sensitivity of the assay with SAM concentrations from 0.195 μ mol to 100 μ mol and plotted a standard curve with a Boltzmann sigmoidal fit (Fig. 4A). Next, we

measured SAM concentration in the 5 knockdown sample versus the 5 controls that were already used for the proteomic experiment. Interestingly, knockdown cells revealed a prominent and highly significant increase in SAM concentration compared with control clones ($p < 10^{-5}$, Fig. 4B).

APP Family Dependent Deregulation of BACE1 and PSEN1—SAM/homocysteine cycle alterations were described to modify DNA methylation status with subsequent down-regulation of *presenilin1* (PSEN1) and *β APP cleaving enzyme 1* (BACE1) at the mRNA level (29). According to those results, we next addressed the expression of BACE and PSEN1 in the knockdown cells versus controls. Indeed, we were able to show a significant down-regulation of PSEN1 in good agreement to the published data (Fig. 4C, $p < 10^{-5}$). In contrast, our results did not support the down-regulation of BACE1 as suggested (29). Contrary, we found a significant ($p < 10^{-3}$) up-regulation in the knockdown cells, which correspond to high levels of SAM (Fig. 4D).

Preclusion of OFF-TARGET Effects for the APP/APLP1/APLP2 Knockdown—Interfering RNAs are able to cross-react with unspecific targets of limited sequence similarity (30). To prevent such unspecific findings, we established a second APP family knockdown model using independent silencing vectors as outlined in the Experimental Procedures part. A significant knockdown could be generated using the same conditions as in the first approach (APP $p < 10^{-4}$; APLP1 $p < 10^{-3}$; APLP2 $p < 10^{-3}$; Fig. 5A). Consistent with the first knockdown model, MAT2A gene expression was significantly silenced ($p < 10^{-4}$, Fig. 5B), whereas PRDX4 mRNA level did not change ($p > 0.05$, Fig. 5C). Finally, qPCR analysis of PSEN1 (Fig. 5D) and BACE1 (Fig. 5E) demonstrated significant differences, which is consistent to the initial APP family knockdown model (PSEN1 $p < 10^{-4}$; BACE1 $p < 10^{-3}$). Thus, off targets effects were not present for the targets studied within this work.

In summary, we identified for the first time MAT2A and PRDX4 as APP-family dependent regulated proteins. In contrast to PRDX4, MAT2A gene expression was also affected. Presumably as a consequence of the MAT2A down-regula-

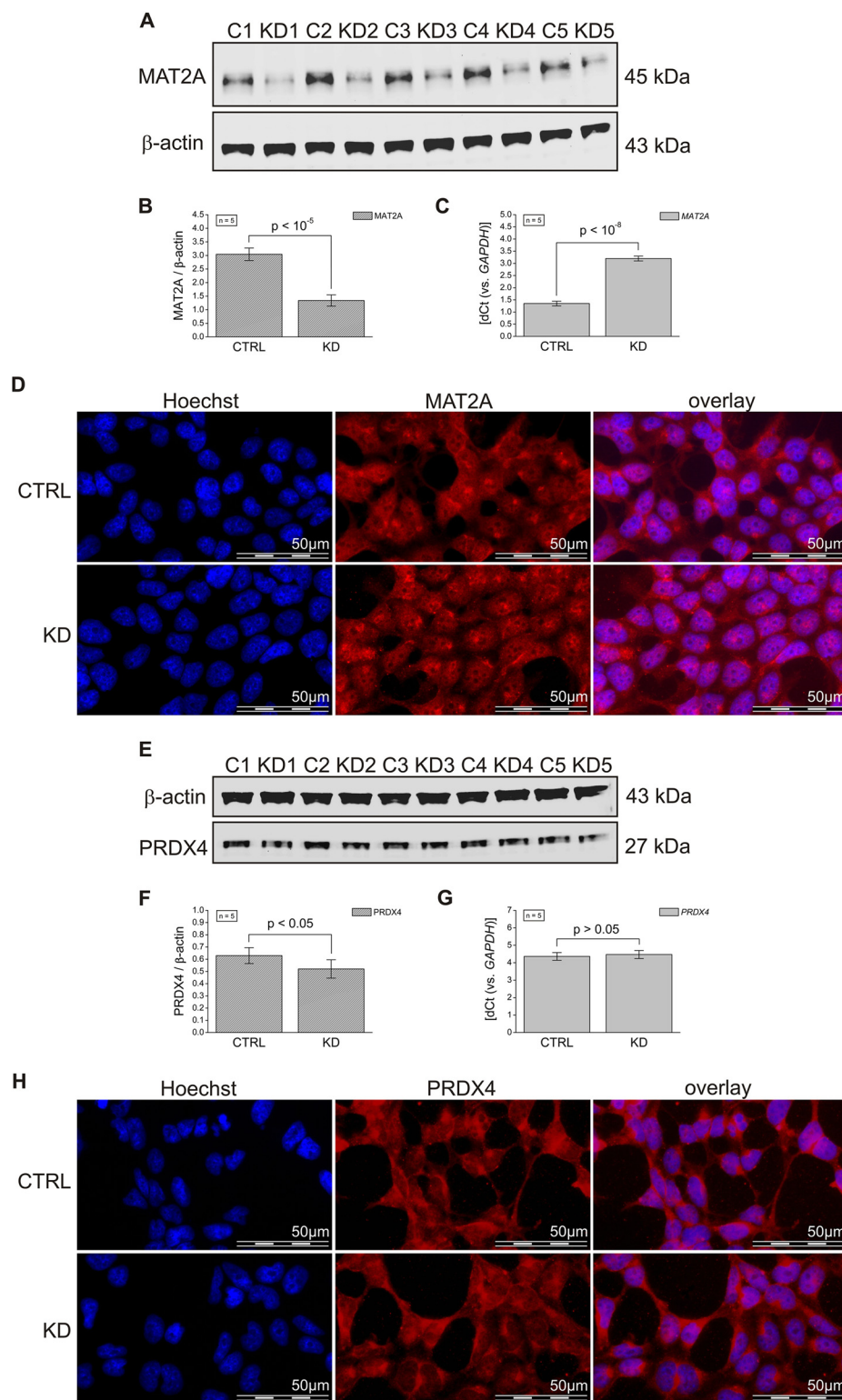


FIG. 3. Validation of MAT2A and PRDX4 down-regulation in APP/APLP1/APLP2 knockdown cells. *A*, Immunoblotting using β -actin as control revealed down-regulation of MAT2A in the knockdown cells versus controls. *B*, Quantification by densitometry demonstrated significance of our findings ($p < 10^{-5}$, 5 knockdown samples versus five control samples ($n = 5$); established by independent transfections with the same shRNAmir constructs). *C*, QPCR analysis of MAT2A indicated down-regulation at the mRNA level, as well ($p < 10^{-8}$, $n = 5$). *D*, Immunofluorescence staining of MAT2A (red) pointed to preferentially nuclear localization without differences between knockdown and control cells (HOECHST (blue) was used as counterstain). *E*, and *F*, PRDX4 immunoblotting validated significant down-regulation at the protein level ($p < 0.05$ according to densitometry, $n = 5$), whereas PRDX4 mRNA level were unaffected in the knockdown cells versus controls ($p > 0.05$, $n = 5$; *G*). *H*, Immunofluorescence analysis of PRDX4 (red) revealed probably preferential ER localization without changes between knockdown and control cells (HOECHST was used as nuclear counterstain).

tion, levels of SAM increase resulting in a deregulation of *BACE1* and *PSEN1* gene expression.

MAT2A Protein Abundance in the Human Frontal Cortex—To evaluate the relevance of our findings for AD pathology, we analyzed protein abundance level of the MAT2A protein using

immunoblotting in human frontal cortex samples from nine AD and 13 control individuals (Fig. 6A). Notably, the densitometric analysis (Fig. 6B) demonstrated significant lower abundance of the MAT2A protein in AD brains ($p < 0.05$), strongly pointing to the relevance of our findings with respect to AD pathology.

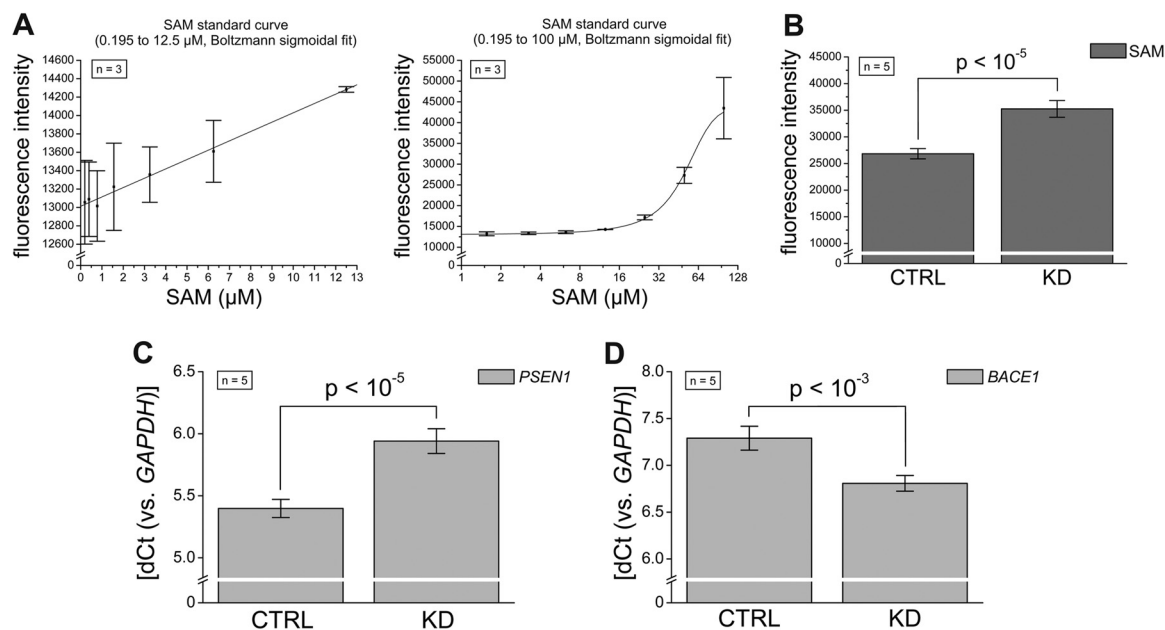


FIG. 4. **Downstream mechanisms of MAT2A regulation.** MAT2A has pivotal enzyme activity for the synthesis of S-adenosylmethionine (SAM). **A**, SAM concentrations ($n = 3$) were assayed using a commercially available kit (see Experimental Procedures) from 0.195 μ mol to 100 μ mol. The SAM standard curve was plotted with a Boltzmann sigmoidal fit. **B**, APP family knockdown clones revealed significant increase in SAM levels compared with controls ($p < 10^{-5}$, $n = 5$). *BACE* and *PSEN1* gene expression changes were suggested as potential downstream effects of SAM. **C**, *PSEN1* mRNA levels were found significantly down-regulated in knockdown cells versus controls ($p < 10^{-5}$, $n = 5$), whereas *BACE1* mRNA levels demonstrated increased levels in the knockdowns versus controls ($p < 10^{-3}$, $n = 5$; **D**).

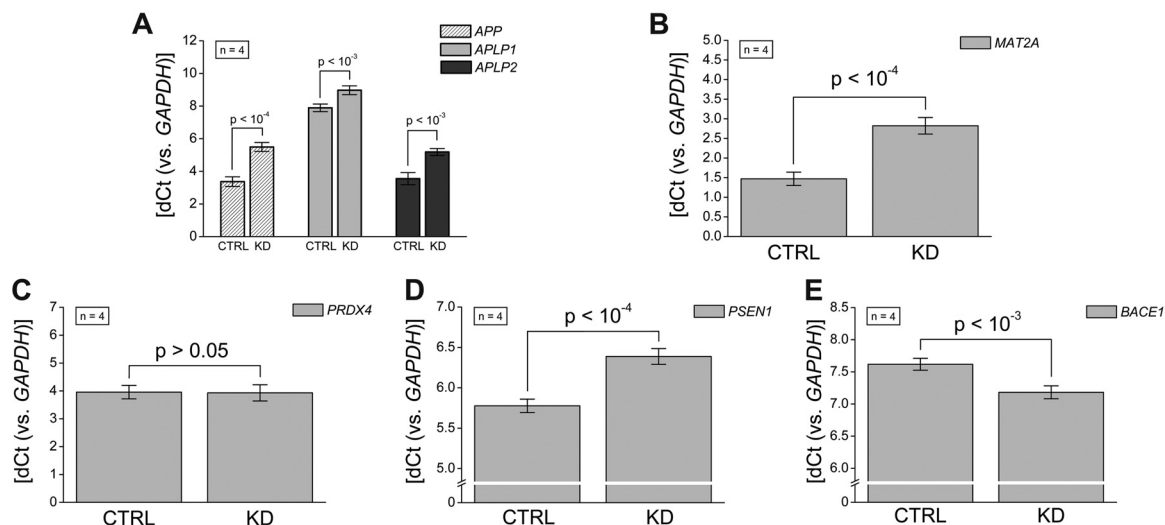


FIG. 5. **Preclusion of OFF TARGET effects for the studied knockdown model.** To exclude unspecific findings, we established another knockdown cell line using a second set of silencing vectors as outlined in the Experimental Procedures part. **A**, Knockdown (KD) of *APP* ($p < 10^{-4}$), *APLP1* ($p < 10^{-3}$), and *APLP2* ($p < 10^{-3}$) was significant when studied in four KD replicates and four controls (CTRL). **B**, Consistently to the first established model, *MAT2A* gene expression was significant increased in the second APP family KD model ($p < 10^{-4}$, $n = 4$). Finally, *PRDX4* expression was unaffected ($p > 0.05$, $n = 4$; **C**), whereas *PSEN1* ($p < 10^{-4}$, $n = 4$; **D**) and *BACE1* ($p < 10^{-3}$, $n = 4$; **E**) expression were significantly changed in well agreement to the initial KD cells.

DISCUSSION

Since the discovery of APP more than 20 years ago, extensive research has been performed analyzing the physiological function of this protein. In mice, APP, APLP1, or APLP2 knockouts revealed a minor phenotype, whereas APLP2 $^{-/-}$ APLP1 $^{-/-}$ and APLP2 $^{-/-}$ APP $^{-/-}$ double mutants were

lethal early after birth. This points to APP family proteins serve essential, but partially redundant, functions (31, 32). Triple APP family knockout mice survive through embryonic development but die shortly after birth (7). In contrast to the double-mutants, the triple APP family knockout mice reveal cranial abnormalities resembling human type 2 lissencephaly. Our

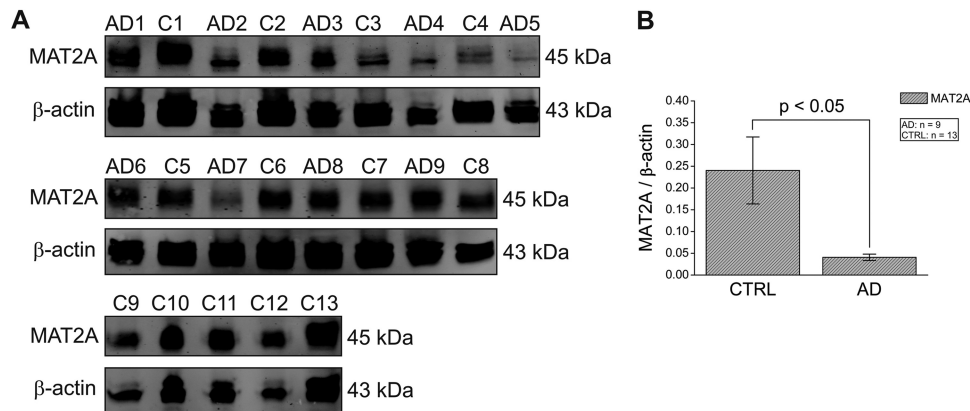


FIG. 6. MAT2A protein abundance in human brain samples. Frontal cortex brain protein lysates from nine AD patients and 13 controls were separated by 1D gel electrophoresis. **A**, Subsequent immunoblotting using anti human MAT2A antibody revealed signals that have been quantified using densitometry (β -actin signal was used for normalization). **B**, Statistical analysis revealed significantly ($p < 0.05$) lower abundance in AD brain samples compared with controls. Error bars correspond to the mean standard error.

state of knowledge in respect to the mechanisms of the APP family is limited due to a lack of cell culture models studied until today. To fill this gap, we established a knockdown model of APP and its highly homologous family members APLP1 and APLP2 in HEK293T cells. Silencing approaches using both siRNA and shRNA constructs failed putatively as a result of the insufficient transfection efficiency, and/or deficient silencing RNA quality. However, transfection of selectable shRNAmir constructs with subsequent puromycin selection resulted in a prominent and significant silencing of all APP family members. This was also true using a second set of silencing vectors targeting an independent RNA sequence of the respective gene. Using a comprehensive proteome approach with subsequent validation and functional experiments, we identified 34 proteins whose expression was severely affected. As outlined by two different pathway analysis tools, regulated proteins were involved in apoptosis signaling, translational processes, methionine metabolism, and others. Subsequent validation experiments revealed MAT2A and PRDX4 as proteins with significant lower abundance in the knockdown cells. MAT2A gene expression was affected in the same manner suggesting a nuclear signaling function from the different compartments in which the APP family is known to be located during their life cycle (33). APP and its family members are characterized by different domains with potential signaling function: the intracellular domain is discussed to submit a nuclear signal caused by a conformational change of its adapter protein FE65. The extracellular sAPP domains were suggested to function as a ligand to specific receptors, and for the sAPP β (respective the sub-fragment N-APP) the DR6 receptor was identified recently (3). According to this present knowledge and the data presented in this work, we suggest a signaling pathway as illustrated in Fig. 7. Further work is needed to elaborate the APP family domain, which is causative for activation of MAT2A.

MAT2A is a central enzyme involved in the generation of SAM, which is important for the methylation of proteins, DNA,

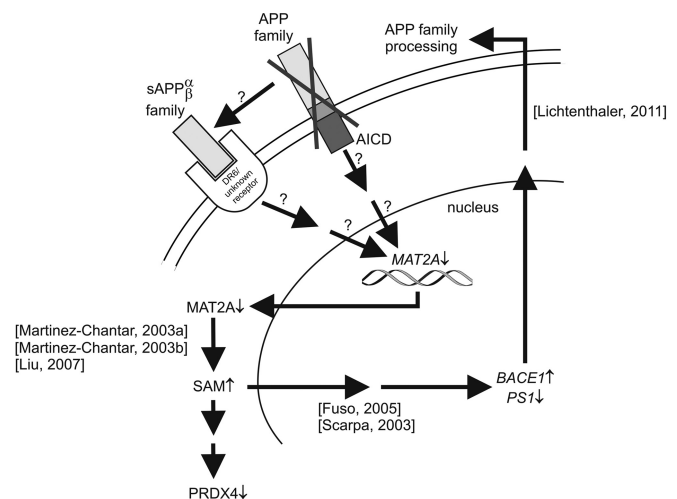


FIG. 7. Hypothetical model for the APP family dependent de-regulation of cellular methylation mechanisms. Knockdown of the APP protein family results in a down-regulation of MAT2A at the RNA and protein level with subsequent SAM elevation. Putatively as a result of increased SAM levels, BACE1 and PSEN1 gene expression are changed as is the PRDX4 protein abundance. APP family signaling might be caused by the corresponding intracellular domains (AICD) or by binding of the extracellular APP family domain to a yet unknown receptor. Notably, sAPP β was recently reported to bind to the death receptor 6. Methylation is an important mechanism for the formation of neurotransmitters like acetylcholine and the level of this neurotransmitter is known to be disturbed in AD. Our findings point to a mechanism that might play a central role for the pathophysiology of AD and might indicate new targets for a therapeutic intervention.

lipids, and the generation of neurotransmitters (34). In mammals, methionine adenosyltransferase (MAT) is encoded by two genes, MAT1A and MAT2A (35). Here, we describe for the first time a significant correlation between the abundance of the APP family and MAT2A expression. MAT2A expression is inversely proportional to SAM levels, whereas MAT1A up-regulation also results in an elevation of SAM (36, 37). Of note,

Liu and co-worker found that silencing MAT2A by small interfering RNA resulted in higher steady-state levels of SAM (37). Consistently, we were able to identify increased SAM levels in the APP/APLP1/APLP2 knockdown cells pointing to a regulatory function of the APP family in SAM levels caused by differential expression of one of the SAM producing enzymes (MAT2A). It is striking that changes of SAM concentration in AD brains were already described in many publications, some of them are decades old (see below). However, a functional connection between SAM and the APP protein family was not described until now. Morrison and colleagues found significantly decreased SAM levels in post-mortem brain samples of AD patients (25). Similarly, SAM was found reduced in the CSF of AD and depressed patients as well (28). Interestingly, SAM treatment of patients in different studies revealed beneficial effects (38–40). As stated in the introduction, our cell culture model might reflect pathological mechanisms of AD in part. Regarding this, results in our model to some extent disagree to the findings in AD patients. However, coherences are further complicated as SAM levels also depend on the abundance and activity of MAT1A in a proportional manner (35). Unfortunately, MAT1A regulation has not been studied in the human brain so far. On the other hand, Selley and co-workers reported a significant increase in the plasma concentrations of SAM in AD patients (41). As SAM concentrations are inversely proportional to MAT2A (35, 37), increased SAM levels would point to lower MAT2A protein abundance. This fits well to our results of lower MAT2A protein abundance in the human frontal cortex of AD patients versus controls and is consistent with findings of decreased MAT2A activity in erythrocytes of patients with dementia disorders (26). Further studies are indicated to unravel the biochemical mechanisms in more detail and to identify that one APP domain, which is responsible for the regulation of MAT2A. Several subdomains are of interest in this context, for example the extracellular domains sAPP α or sAPP β as well as the APP intracellular domain (AICD). While there is a reduction of sAPP α in AD, the elevated amyloidogenic cleavage causes increased levels of sAPP β . In addition, AICD signaling predominantly occurs through the amyloidogenic processing (42). In the APP family knockdown model all of these domains are missing. Thus, the model is able to indicate AD relevant pathways, but it is less applicable to predict the full course of regulation in AD. As a consequence, our results in human samples point to the relevance of APP family dependent regulation of MAT2A, subsequent SAM level changes, and disturbance of the cellular methylation mechanisms for the pathology of AD. Down-regulation of MAT2A might correspond to a compensatory effect of stressed neurons in order to ensure high levels of SAM for sufficient neurotransmitter generation. On the other hand, low SAM levels resulting from a deregulation of the cellular methylation machinery might evoke cellular stress, and an association between SAM and the superoxide dismutase activity was reported recently (43). Additionally, the

down-regulation of PRDX4 was suggested to facilitate cell death (44). Consistently, we were able to measure lower PRDX4 protein abundance in the triple APP/APLP1/APLP2 knockdown cells pointing to a cellular stress condition, which is a central hallmark of AD (45). Notably, APP cleavage and subsequent generation of β -amyloid generates oxidative stress, and membrane lipid peroxidation in particular (46). Lipid membranes belong to the most vulnerable cellular components to oxidative stress, and membranes in susceptible regions of the brain are compositionally distinct from membranes in other tissues (45). Similarly, antioxidant therapies lowering oxidative stress in AD pathogenesis are under discussion (47).

Some findings of SAM-dependent deregulation of *BACE* and *PSEN1* gene expression (29, 48) motivated us to study these APP processing enzymes by qPCR. Indeed, *BACE1* expression was significantly up-regulated in the knockdown cells, whereas *PSEN1* was down-regulated. This suggests an APP self-regulatory mechanism (Fig. 7) since both enzymes are pivotally involved in the cleavage of APP (49). The expression changes in APP family cleaving enzymes might correspond to a cellular mechanism compensating low levels of the APP family, especially by elevating levels of the β -secretase cleavage fragments, sAPP β (representative for the APP family) and CTF β (c-terminal fragment). The concomitant down-regulation of *PSEN1* suggests a compensatory function for the sAPP β fragment. Certainly, the ultimate answer to this hypothesis will require additional examinations. Nevertheless, the link of the APP family knockdown and down-regulation of a central enzyme responsible for the generation of a pivotal methylation donor appeared to be highly attractive because SAM is essential for the transmethylation of neurotransmitters such as adrenalin and acetylcholine (34), the latter plays a central role in AD (50). In detail, SAM is essential for the generation of phosphatidylcholine, which is a precursor of choline for acetylcholine synthesis (51). It is striking that the phenotype of APP/APLP2 knockout mice was reported to overlap, to a large degree, with mice deficient in choline acetyltransferase (9). Our data suggest that the APP family dependent regulation of SAM might be responsible for the proper generation of acetylcholine. This hypothesis fits to reports of disturbed synaptic vesicle density and synaptic failure in APP/APLP2 knockout mice (9, 52) as well as to cranial abnormalities (7) putatively resulting from cholinergic neuron dysfunction. Cholinergic decline is central hallmark of AD manifesting the cholinergic hypothesis. Many drugs like acetylcholinesterase inhibitors have been developed and are in development to improve memory as well as other cognitive functions (53). In this work, elaborated mechanisms of APP family dependent regulation of SAM might deliver new targets for a pharmacological intervention.

Taken together, our data demonstrate a central role for the APP protein family in the regulation of cellular meth-

ylation caused by MAT2A and subsequent SAM deregulation. This deregulation seems to be associated with oxidative stress and gene expression changes of the APP cleaving proteases PSEN1 and BACE1. Methylation is an important modification for DNA and for proteins, and is also essential for the production of neurotransmitters like acetylcholine. The cholinergic system is known to be severely affected in AD. This hypothetical model not only demonstrates a crucial mechanism for the APP family under physiological conditions, but also for the pathophysiology of AD. Notably, our data also demonstrate significant lower MAT2A protein abundance in human frontal cortex brain samples from patients suffering from AD. The connection of the APP family to MAT2A, might highlight new targets for a therapeutic intervention helping patients suffering from AD or prestages.

Acknowledgments—We thank Prof. Jens Wiltfang (Clinic for Psychiatry and Psychotherapy, University Duisburg-Essen, Germany) for providing the anti-human full length APP antibody used in this work.

* This work was funded by FoRUM (Forschungsförderung Ruhr-Universität Bochum Medizinische Fakultät) AZ-F616-2008 and AD F680-2009. We thank the federal state North Rhine-Westphalia for funding within the project PURE.

‡ To whom correspondence should be addressed: Functional Proteomics, Medizinisches Proteom-Center, Ruhr-University Bochum, D-44801 Bochum, Germany. Tel.: +49 234 32 28444; Fax: +49 234 32 14496; E-mail: thorsten.t.mueller@rub.de.

** Both authors contributed equally.

The authors declare that they have no conflict of interest.

REFERENCES

- Zheng, H., and Koo, E. H. (2006) The amyloid precursor protein: beyond amyloid. *Mol. Neurodegener.* **1**, 5
- Müller, T., Meyer, H. E., Egensperger, R., and Marcus, K. (2008) The amyloid precursor protein intracellular domain (AICD) as modulator of gene expression, apoptosis, and cytoskeletal dynamics-Relevance for Alzheimer's disease. *Prog. Neurobiol.* **85**, 393–406
- Nikolaev, A., McLaughlin, T., O'Leary, D. D., and Tessier-Lavigne, M. (2009) APP binds DR6 to trigger axon pruning and neuron death via distinct caspases. *Nature* **457**, 981–989
- Müller, T., Concannon, C. G., Ward, M. W., Walsh, C. M., Timmerier, A. L., Tribl, F., Kogel, D., Pohn, J. H., and Egensperger, R. (2007) Modulation of Gene Expression and Cytoskeletal Dynamics by the Amyloid Precursor Protein Intracellular Domain (AICD). *Mol. Biol. Cell* **18**, 201–210
- Furukawa, K., Sopher, B. L., Rydel, R. E., Begley, J. G., Pham, D. G., Martin, G. M., Fox, M., and Mattson, M. P. (1996) Increased activity-regulating and neuroprotective efficacy of alpha-secretase-derived secreted amyloid precursor protein conferred by a C-terminal heparin-binding domain. *J. Neurochem.* **67**, 1882–1896
- Eggert, S., Paliga, K., Soba, P., Evin, G., Masters, C. L., Weidemann, A., and Beyreuther, K. (2004) The proteolytic processing of the amyloid precursor protein gene family members APLP-1 and APLP-2 involves alpha-, beta-, gamma-, and epsilon-like cleavages: modulation of APLP-1 processing by n-glycosylation. *J. Biol. Chem.* **279**, 18146–18156
- Hermes, J., Anliker, B., Heber, S., Ring, S., Fuhrmann, M., Kretschmar, H., Sisodia, S., and Müller, U. (2004) Cortical dysplasia resembling human type 2 lissencephaly in mice lacking all three APP family members. *EMBO J.* **23**, 4106–4115
- Ring, S., Weyer, S. W., Kilian, S. B., Waldron, E., Pietrzik, C. U., Filippov, M. A., Hermes, J., Buchholz, C., Eckman, C. B., Korte, M., Wolf, D. P., and Müller, U. C. (2007) The secreted beta-amyloid precursor protein ectodomain APPs alpha is sufficient to rescue the anatomical, behavioral, and electrophysiological abnormalities of APP-deficient mice. *J. Neurosci.* **27**, 7817–7826
- Wang, P., Yang, G., Mosier, D. R., Chang, P., Zaidi, T., Gong, Y. D., Zhao, N. M., Dominguez, B., Lee, K. F., Gan, W. B., and Zheng, H. (2005) Defective neuromuscular synapses in mice lacking amyloid precursor protein (APP) and APP-Like protein 2. *J. Neurosci.* **25**, 1219–1225
- Bergmans, B. A., Shariati, S. A., Habets, R. L., Verstreken, P., Schoonjans, L., Müller, U., Dotti, C. G., and De, S. B. (2010) Neurons generated from APP/APLP1/APLP2 triple knockout embryonic stem cells behave normally in vitro and in vivo: lack of evidence for a cell autonomous role of the amyloid precursor protein in neuronal differentiation. *Stem Cells* **28**, 399–406
- Schrenk-Siemens, K., Perez-Alcala, S., Richter, J., Lacroix, E., Rahuel, J., Korte, M., Müller, U., Barde, Y. A., and Bibel, M. (2008) Embryonic stem cell-derived neurons as a cellular system to study gene function: lack of amyloid precursor proteins APP and APLP2 leads to defective synaptic transmission. *Stem Cells* **26**, 2153–2163
- Lannfelt, L., Basun, H., Wahlund, L. O., Rowe, B. A., and Wagner, S. L. (1995) Decreased alpha-secretase-cleaved amyloid precursor protein as a diagnostic marker for Alzheimer's disease. *Nat. Med.* **1**, 829–832
- Nakaya, T., and Suzuki, T. (2006) Role of APP phosphorylation in FE65-dependent gene transactivation mediated by AICD. *Genes Cells* **11**, 633–645
- Livak, K. J., and Schmittgen, T. D. (2001) Analysis of relative gene expression data using real-time quantitative PCR and the 2(-Delta Delta C(T)) Method. *Methods* **25**, 402–408
- Müller, T., Loosse, C., Schrötter, A., Schnabel, A., Helling, S., Egensperger, R., and Marcus, K. (2011) The AICD interacting protein DAB1 is up-regulated in Alzheimer frontal cortex brain samples and causes deregulation of proteins involved in gene expression changes. *Curr. Alzheimer Res.* **8**, 573–582
- Spitzer, P., Klafki, H. W., Blennow, K., Buee, L., Esselmann, H., Herruka, S. K., Jimenez, C., Klivenyi, P., Lewczuk, P., Maler, J. M., Markus, K., Meyer, H. E., Morris, C., Müller, T., Otto, M., Parnetti, L., Soininen, H., Schraen, S., Teunissen, C., Vecsei, L., Zetterberg, H., and Wiltfang, J. (2010) cNEUPRO: novel biomarkers for neurodegenerative diseases. *Int. J. Alzheimers. Dis.* pii, 548145
- Reidegeld, K. A., Eisenacher, M., Kohl, M., Chamrad, D., Korting, G., Blüggel, M., Meyer, H. E., and Stephan, C. (2008) An easy-to-use Decoy Database Builder software tool, implementing different decoy strategies for false discovery rate calculation in automated MS/MS protein identifications. *Proteomics* **8**, 1129–1137
- Müller, T., Schrötter, A., Loosse, C., Helling, S., Stephan, C., Ahrens, M., Uszkoreit, J., Eisenacher, M., Meyer, H. E., and Marcus, K. (2011) Sense and nonsense of pathway analysis software in proteomics. *J. Proteome Res.* **10**, 5398–5408
- Benjamini, Y., and Hochberg, Y. (1995) Controlling the false discovery rate: a practical and powerful approach to multiple testing. *J. Roy. Stat. Soc. B* **57**, 289–300
- Braak, H., and Braak, E. (1991) Neuropathological staging of Alzheimer-related changes. *Acta Neuropathol.* **82**, 239–259
- Mirra, S. S., Heyman, A., McKeel, D., Sumi, S. M., Crain, B. J., Brownlee, L. M., Vogel, F. S., Hughes, J. P., van Belle, G., and Berg, L. (1991) The Consortium to Establish a Registry for Alzheimer's Disease (CERAD). Part II. Standardization of the neuropathologic assessment of Alzheimer's disease. *Neurology* **41**, 479–486
- Katoh, Y., Ikura, T., Hoshikawa, Y., Tashiro, S., Ito, T., Ohta, M., Kera, Y., Noda, T., and Igarashi, K. (2011) Methionine adenosyltransferase II serves as a transcriptional corepressor of Maf oncoprotein. *Mol. Cell* **41**, 554–566
- Panza, F., Frisardi, V., Capurso, C., D'Introno, A., Colacicco, A. M., Vendemiale, G., Capurso, A., and Solfrizzi, V. (2009) Possible role of S-adenosylmethionine, S-adenosylhomocysteine, and polyunsaturated fatty acids in predementia syndromes and Alzheimer's disease. *J. Alzheimers. Dis.* **16**, 467–470
- Kim, S. H., Fountoulakis, M., Cairns, N., and Lubec, G. (2001) Protein levels of human peroxiredoxin subtypes in brains of patients with Alzheimer's disease and Down syndrome. *J. Neural Transm.* **61**, 223–235
- Morrison, L. D., Smith, D. D., and Kish, S. J. (1996) Brain S-adenosylmethionine levels are severely decreased in Alzheimer's disease. *J. Neurochem.* **67**, 1328–1331
- Gomes, Trolin, C., Regland, B., and Oreland, L. (1995) Decreased methio-

- nine adenosyltransferase activity in erythrocytes of patients with dementia disorders. *Eur. Neuropsychopharmacol.* **5**, 107–114
27. Trolin, C. G., Löfberg, C., Trolin, G., and Orelund, L. (1994) Brain ATP:L-methionine S-adenosyltransferase (MAT), S-adenosylmethionine (SAM) and S-adenosylhomocysteine (SAH): regional distribution and age-related changes. *Eur. Neuropsychopharmacol.* **4**, 469–477
28. Bottiglieri, T., Godfrey, P., Flynn, T., Carney, M. W., Toone, B. K., and Reynolds, E. H. (1990) Cerebrospinal fluid S-adenosylmethionine in depression and dementia: effects of treatment with parenteral and oral S-adenosylmethionine. *J. Neurol. Neurosurg. Psychiatry* **53**, 1096–1098
29. Fuso, A., Seminara, L., Cavallaro, R. A., D'Anselmi, F., and Scarpa, S. (2005) S-adenosylmethionine/homocysteine cycle alterations modify DNA methylation status with consequent deregulation of PS1 and BACE and beta-amyloid production. *Mol. Cell Neurosci.* **28**, 195–204
30. Jackson, A. L., Bartz, S. R., Schelter, J., Kobayashi, S. V., Burchard, J., Mao, M., Li, B., Cavet, G., and Linsley, P. S. (2003) Expression profiling reveals off-target gene regulation by RNAi. *Nat. Biotechnol.* **21**, 635–637
31. von Koch, C. S., Zheng, H., Chen, H., Trumbauer, M., Thinakaran, G., van der Ploeg, L. H., Price, D. L., and Sisodia, S. S. (1997) Generation of APLP2 KO mice and early postnatal lethality in APLP2/APP double KO mice. *Neurobiol. Aging* **18**, 661–669
32. Heber, S., Herms, J., Gajic, V., Hainfellner, J., Aguzzi, A., Rüdliche, T., von Kretschmar, H., von Koch, C., Sisodia, S., Tremml, P., Lipp, H. P., Wolfer, D. P., and Müller, U. (2000) Mice with combined gene knock-outs reveal essential and partially redundant functions of amyloid precursor protein family members. *J. Neurosci.* **20**, 7951–7963
33. Sannerud, R., and Annaert, W. (2009) Trafficking, a key player in regulated intramembrane proteolysis. *Semin. Cell Dev. Biol.* **20**, 183–190
34. Miller, A. L. (2008) The methylation, neurotransmitter, and antioxidant connections between folate and depression. *Altern. Med. Rev.* **13**, 216–226
35. Martinez-Chantar, M. L., Latasa, M. U., Varela-Rey, M., Lu, S. C., Garcia-Trevijano, E. R., Mato, J. M., and Avila, M. A. (2003) L-methionine availability regulates expression of the methionine adenosyltransferase 2A gene in human hepatocarcinoma cells: role of S-adenosylmethionine. *J. Biol. Chem.* **278**, 19885–19890
36. Martinez-Chantar, M. L., Garcia-Trevijano, E. R., Latasa, M. U., Martin-Duce, A., Fortes, P., Caballeria, J., Avila, M. A., and Mato, J. M. (2003) Methionine adenosyltransferase II beta subunit gene expression provides a proliferative advantage in human hepatoma. *Gastroenterology* **124**, 940–948
37. Liu, Q., Wu, K., Zhu, Y., He, Y., Wu, J., and Liu, Z. (2007) Silencing MAT2A gene by RNA interference inhibited cell growth and induced apoptosis in human hepatoma cells. *Hepatol. Res.* **37**, 376–388
38. Cohen, B. M., Satlin, A., and Zubenko, G. S. (1988) S-adenosyl-L-methionine in the treatment of Alzheimer's disease. *J. Clin. Psychopharmacol.* **8**, 43–47
39. Knopman, D., and Patterson, M. (2001) An open-label, 24-week pilot study of the methyl donor betaine in Alzheimer disease patients. *Alzheimer Dis. Assoc. Disord.* **15**, 162–165
40. Shea, T. B., and Chan, A. (2008) S-adenosyl methionine: a natural therapeutic agent effective against multiple hallmarks and risk factors associated with Alzheimer's disease. *J. Alzheimers. Dis.* **13**, 67–70
41. Selley, M. L. (2007) A metabolic link between S-adenosylhomocysteine and polyunsaturated fatty acid metabolism in Alzheimer's disease. *Neurobiol. Aging* **28**, 1834–1839
42. Goodger, Z. V., Rajendran, L., Trutzel, A., Kohli, B. M., Nitsch, R. M., and Konietzko, U. (2009) Nuclear signaling by the APP intracellular domain occurs predominantly through the amyloidogenic processing pathway. *J. Cell Sci.* **122**, 3703–3714
43. Cavallaro, R. A., Fuso, A., Nicolai, V., and Scarpa, S. (2010) S-adenosylmethionine prevents oxidative stress and modulates glutathione metabolism in TgCRND8 mice fed a B-vitamin deficient diet. *J. Alzheimers. Dis.* **20**, 997–1002
44. Wang, H. Q., Du, Z. X., Liu, B. Q., Gao, Y. Y., Meng, X., Guan, Y., and Zhang, H. Y. (2009) TNF-related apoptosis-inducing ligand suppresses PRDX4 expression. *FEBS Lett.* **583**, 1511–1515
45. Axelsen, P. H., Komatsu, H., and Murray, I. V. (2011) Oxidative stress and cell membranes in the pathogenesis of Alzheimer's disease. *Physiology* **26**, 54–69
46. Mattson, M. P., and Pedersen, W. A. (1998) Effects of amyloid precursor protein derivatives and oxidative stress on basal forebrain cholinergic systems in Alzheimer's disease. *Int. J. Dev. Neurosci.* **16**, 737–753
47. Lee, H. P., Zhu, X., Casadesus, G., Castellani, R. J., Nunomura, A., Smith, M. A., Lee, H. G., and Perry, G. (2010) Antioxidant approaches for the treatment of Alzheimer's disease. *Expert. Rev. Neurother.* **10**, 1201–1208
48. Scarpa, S., Fuso, A., D'Anselmi, F., and Cavallaro, R. A. (2003) Presenilin 1 gene silencing by S-adenosylmethionine: a treatment for Alzheimer disease? *FEBS Lett.* **541**, 145–148
49. Lichtenthaler, S. F., Haass, C., and Steiner, H. (2011) Regulated intramembrane proteolysis—lessons from amyloid precursor protein processing. *J. Neurochem.* **117**, 779–796
50. Schliebs, R., and Arendt, T. (2011) The cholinergic system in aging and neuronal degeneration. *Behav. Brain Res.* **221**, 555–563
51. Blusztajn, J. K., Liscovitch, M., Mauron, C., Richardson, U. I., and Wurtman, R. J. (1987) Phosphatidylcholine as a precursor of choline for acetylcholine synthesis. *J. Neural Transm. Suppl.* **24**, 247–259
52. Yang, G., Gong, Y. D., Gong, K., Jiang, W. L., Kwon, E., Wang, P., Zheng, H., Zhang, X. F., Gan, W. B., and Zhao, N. M. (2005) Reduced synaptic vesicle density and active zone size in mice lacking amyloid precursor protein (APP) and APP-like protein 2. *Neurosci. Lett.* **384**, 66–71
53. Martorana, A., Esposito, Z., and Koch, G. (2010) Beyond the cholinergic hypothesis: do current drugs work in Alzheimer's disease? *CNS. Neurosci. Ther.* **16**, 235–245